

APPLICATION OF IN-SITU DIFFRACTION EXPERIMENTS TO UNDERSTAND NONEQUILIBRIUM PHASE TRANSFORMATIONS IN STRUCTURAL ALLOYS

S. S. Babu¹, J. W. Elmer², E. D. Specht¹, J. M. Vitek¹, S. A. David¹

¹Metals and Ceramics Division, Oak Ridge National Laboratory
Oak Ridge, Tennessee, 37831, USA

²Chemistry and Materials Science Department, Lawrence Livermore National Laboratory
Livermore, CA 94551, USA

Keywords: In-situ Time-Resolved X-ray diffraction, Nonequilibrium Phase Transformation,
Steels, Bainitic Transformation

Abstract

It has been a challenge to measure in-situ phase transformation kinetics in structural alloys under rapid thermal cycles with good time resolution in the past. However, by using high-brightness synchrotron sources that deliver sufficient photon fluxes, in-situ time-resolved X-ray diffraction measurements with millisecond time-resolution are now possible. This technique was used to track nonequilibrium austenite formation in a Fe-C-Al-Mn steel weld during solidification. This solidification mode is contrary to the equilibrium ferrite solidification mode. Subsequent to solidification, splitting of austenite diffraction peaks with two different lattice parameters was observed during cooling. Continued cooling led to the decomposition of low-volume austenite into bainite first which was followed by the decomposition of large-volume austenite to martensite. A similar phenomenon of austenite splitting and subsequent transformation of low-volume austenite first was also observed in a high-carbon steel before bainitic transformation.

Introduction

Theoretical models based on local-equilibrium [1] at the interface have been developed for describing kinetics of phase changes in structural alloys. In the past decade, these models have been applied to describe phase changes that occur during welding and heat-treatment of steels, aluminum alloys, and nickel base superalloys [2–6]. It is also well known that, under certain conditions, the microstructure evolution occurs under nonequilibrium conditions. These nonequilibrium conditions include departure from local-equilibrium at the interface leading to solute trapping, paraequilibrium conditions [7], selection of nonequilibrium phases and different decomposition paths. There have been attempts to describe these phenomena using modified models [8,9,10]. However, there is a critical need to compare these calculations with in-situ measurements of phase changes under realistic thermomechanical conditions.

In this regard, time-resolved in-situ synchrotron [11–20] and neutron [21,22] scattering techniques are ideal. With the development of brighter and high-flux synchrotron [23,24,25] and neutron sources [26,27,28], it is possible to interrogate the materials during complex thermomechanical cycles with a time resolution of milliseconds or minutes, respectively. The application of the synchrotron and neutron tools for conventional heat-treatments is not new [29]. However, Elmer et al [11–13] pioneered the use of this technique to track phase transformation

in welds. Elmer and co-workers employed time-resolved X-ray diffraction (TRXRD) and also spatially resolved X-ray diffraction (SRXRD) to understand the phase evolution in the welds made on steels and titanium alloys. In this paper, the power of this technique to track non-equilibrium microstructure evolution is reviewed with two examples.

In the first example, the microstructure evolution in the heat-affected-zone (HAZ) and the fusion zone (FZ) of a Fe-C-Al-Mn steel weld was characterized. The measured phase transformation kinetics in the HAZ was compared with calculations from diffusion controlled transformation models [30]. To evaluate the phase transformation kinetics in the fusion zone, the interface response function models [31] were used.

In the second example, the transformation kinetics of austenite to a high-strength bainitic microstructure in a high-carbon steel was measured. In earlier research, Caballero et al [32] measured the transformation kinetics by detailed heat-treatment and optical metallography. The microstructure following isothermal transformation is a mixture of bainitic ferrite and carbon-enriched retained austenite [33]. The measured transformation kinetics was evaluated with computational thermodynamic and kinetic calculations.

Experimentation

In-situ Welding Experiment

TRXRD measurements during welding were performed on a 31-pole wiggler 10-2 beam line [34] at Stanford Synchrotron Radiation Laboratory with the Stanford Positron Electron Accumulation Ring operating at an electron energy of 3.0 GeV and an injection current of ~ 100 mA. The focused monochromatic beam was passed through a tungsten pinhole to render a sub-millimeter beam on the sample at an incident angle of $\sim 25^\circ$. A 730- μm -diam pinhole defines the beam size on the sample. Photon energy of 12.0 keV ($\lambda = 0.1033$ nm) was chosen to maximize the number of peaks diffracting into the 2θ window of the X-ray detector. The diffraction intensities at various 2θ positions were monitored continuously and in real time using a 5 cm-long photodiode array covering a 2θ range of approximately 30° at 0.05-s time resolution. The experimental setup is shown in Fig. 1 and more details can be found in references 11–15.

In-situ Heat Treatment Experiment

The beam line X33-BM-C at the Advanced Photon Source (Argonne, Illinois) with bending magnet synchrotron radiation was used for heat-treatment study. A double-crystal Si(111) monochromator selected and sagittally focused to 30 keV X rays. At this energy, the penetration depth in steel is 0.16 mm.

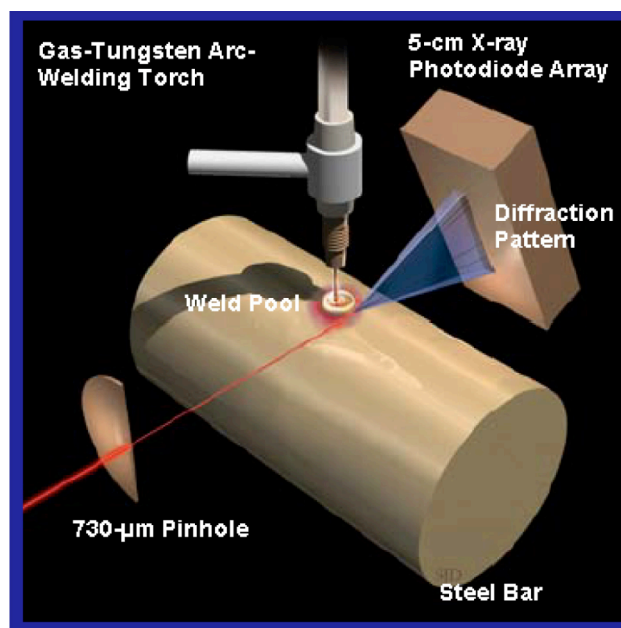


Fig. 1. Schematic illustration of gas-tungsten arc-spot welding experimental set-up for performing time-resolved X-ray diffraction measurement in the fusion zone and the heat-affected-zone of the weld is shown.

Slits defined a beam 0.25 mm high and 1.0 mm wide on the sample. X-rays were incident on the sample surface at a glancing angle of 5°. A schematic illustration of the experiment and a typical diffraction image is shown in Fig. 2. Diffracted X-rays were measured using a 1024x1024 pixel, Peltier-cooled, 16 bit CCD detector. The minimum time resolution that can be attained in this set up without deterioration of signal to noise ratio was found to be 3 s. Therefore, in the early stages of transformation the time resolution was set to 3 s and at the later stages of transformation the time resolution was increased to 34 s to minimize the computer memory requirements. The powder diffraction rings were integrated to give 1D scans of intensity versus interplanar spacing [35]. Further details of the experiment can be found in the published reference [36].

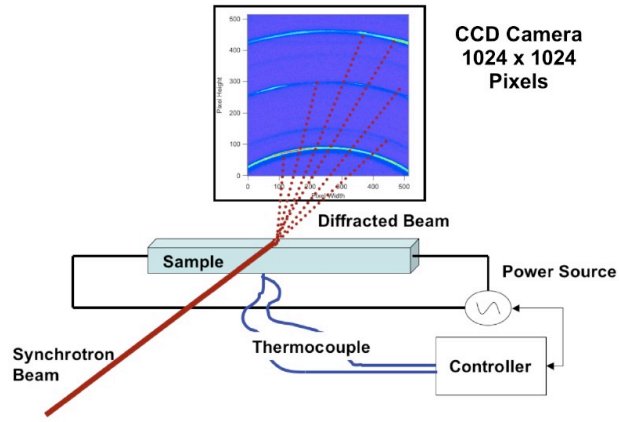


Fig. 2 Schematic illustration of heat-treatment experimental setup and time-resolved X-ray diffraction measurement using CCD camera is shown. The uniform hot-zone width in the middle of the sample is approximately 15 mm and exceeds the size of the incident synchrotron beam (0.25 mm high and 1.0 mm wide).

Computational Thermodynamic and Kinetic Calculations

The equilibrium thermodynamic phase evolution in the HAZ was predicted by using ThermoCalc® software [1, 37] version Q with the solid solution database [38]. The calculations considered equilibrium between liquid, ferrite (**bcc**), austenite (**fcc**), and cementite (**Fe₃C**). In addition to equilibrium thermodynamic calculations, diffusion controlled growth of ferrite into austenite during the weld heating was simulated by using DICTRA software [1]. In these calculations, SSOL solid solution thermodynamic databases and standard (MOB) mobility databases were used.

Since the current research in Fe-C-Al-Mn steel pertains to the weld solidification, it is necessary to consider nonequilibrium weld solidification that occurs due to increased liquid-solid interface velocities under rapid cooling conditions. In this work, a previously published interface-response function model [9,31] that predicts the solid-liquid interface temperature as a function of velocity is used, taking into account non-equilibrium partitioning [39,40,41], and the selection of a nonequilibrium primary phase and changes in liquid-solid interface morphology [42,43].

Results and Discussions

Nonequilibrium Microstructure Evolution in Fe-C-Al-Mn steel Welds

Self-shielded flux-cored arc steel welds contain high residual levels of aluminum (> 1 wt.%). This is mainly because this welding process does not use gaseous shielding. This leads to pick up of oxygen and nitrogen from the atmosphere. Therefore, this process relies on intentional addition of aluminum to deoxidize and denitride the welds. The bulk chemical composition of the steel studied in this work is Fe-0.23C-0.5Mn-1.7Al-0.28Si – 0.02 Ni – 0.003 Ti – 0.006 O – 0.064N (wt.%). The presence of high aluminum forces these welds to solidify as δ -ferrite under conventional weld conditions. In addition, the excess aluminum stabilizes the δ -ferrite and

avoids the formation of 100% austenite during cooling. The small amount of austenite that forms in the interdendritic regions decomposes either to bainite or pearlite depending upon the cooling rate. As a result, the fusion zone inherits the columnar δ -ferrite microstructure to the room temperature as shown in Fig. 3a. This microstructure was found to be in agreement with computational thermodynamic and kinetic calculations [2].

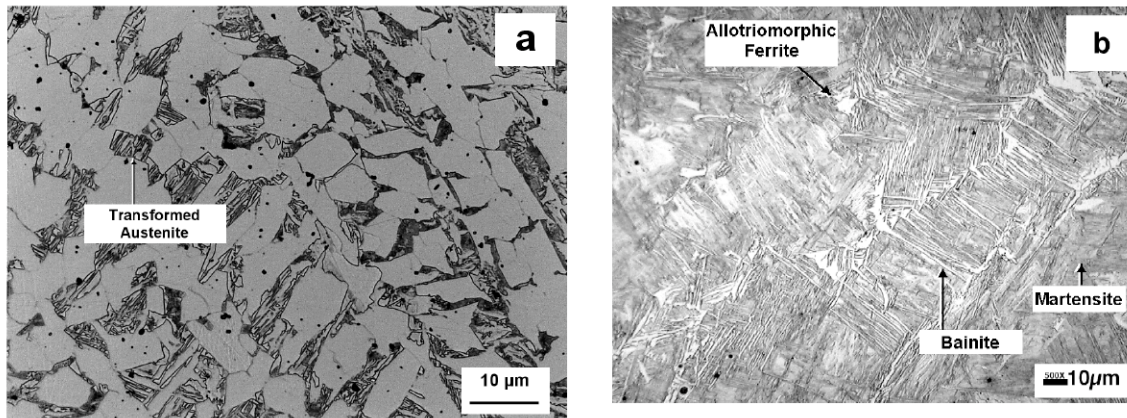


Fig. 3: Microstructures of fusion zone with composition Fe-0.23C-0.5Mn-1.7Al-0.28Si – 0.02 Ni – 0.003 Ti – 0.006 O – 0.064N (wt.%) for (a) slow weld cooling and (b) rapid weld cooling conditions show different microstructures.

However, in certain rapid weld cooling conditions, the microstructure of the same steels contained no residual columnar δ -ferrite. Instead, the microstructure contained allotriomorphic ferrite, bainite and martensite [see Fig. 3b], similar to that expected to form from 100% austenite microstructure. The absence of columnar δ -ferrite in these rapidly cooled welds could be explained theoretically using two paths of phase evolution. In the first path, the liquid transforms to 100% δ -ferrite. Subsequently, the δ -ferrite transforms to 100% austenite by massive transformation and later on this austenite transforms to a mixture of allotriomorphic ferrite, bainite and martensite during subsequent cooling. In the second path the liquid transforms to 100% austenite by nonequilibrium solidification and then transforms to a mixture of allotriomorphic ferrite, bainite and martensite during subsequent cooling. Since the final microstructure does not yield any information on the phase transformations that occur at high temperature, it is impossible to conclude which is the correct microstructure evolution path. Therefore, we used in-situ TRXRD to track the phase evolution during weld cooling.

Dynamics of Phase Changes in the Heat-Affected-Zone

In order to understand the phase evolution in the fusion zone, it is important to first understand the phase evolution in the heat-affected-zone of these welds. This is because the phases that are present in the HAZ at high temperature will influence the first solidifying grains that grow epitaxially into the fusion zone. To observe the HAZ phase transformations, TRXRD measurements were made in the HAZ of a Fe-C-Al-Mn steel during rapid heating and cooling spot welding conditions. In this experiment, the welding arc was on for 17 seconds and then was shut off abruptly. This condition leads to a fairly slow heating and a fast cooling rate. The diffraction measurements were made at a time-resolution of 0.05 seconds for the whole duration of the weld as the steel heats and cools.

The measured diffraction intensity of austenite and ferrite as a function of time is presented in Fig. 4a in an image format. The darker regions correspond to high intensity of diffraction peaks and the grey color corresponds to the background intensity. The image shows the positions of

the **bcc** (110) (ferrite) and **fcc** (111) (austenite) peaks at different times. For the first 17 seconds, the data show the heating-up portion of the weld thermal cycle. Initially, the lattice parameter of ferrite increases (2θ decreases) as the temperature increases. At a critical temperature, the formation of austenite can be inferred from the appearance of **fcc** (111) diffraction peaks. Continued heating leads to a reduction of **bcc** (110) peak intensity. At about 17 seconds into the experiment, the arc was shut off, creating rapid cooling conditions and decomposition of austenite. The area fractions of the peaks were used to evaluate the kinetics of ferrite decomposition during heating and growth during cooling as shown in Fig. 4b. Interestingly, this result showed that the austenite formation was not complete, even at high-temperature, indicating the high-stability of ferrite phase in these steels. Interestingly, the ferrite fraction is not restored due the sluggish transformation kinetics during cooling. In the next step, the observed result was evaluated with computational thermodynamic and kinetic calculations.

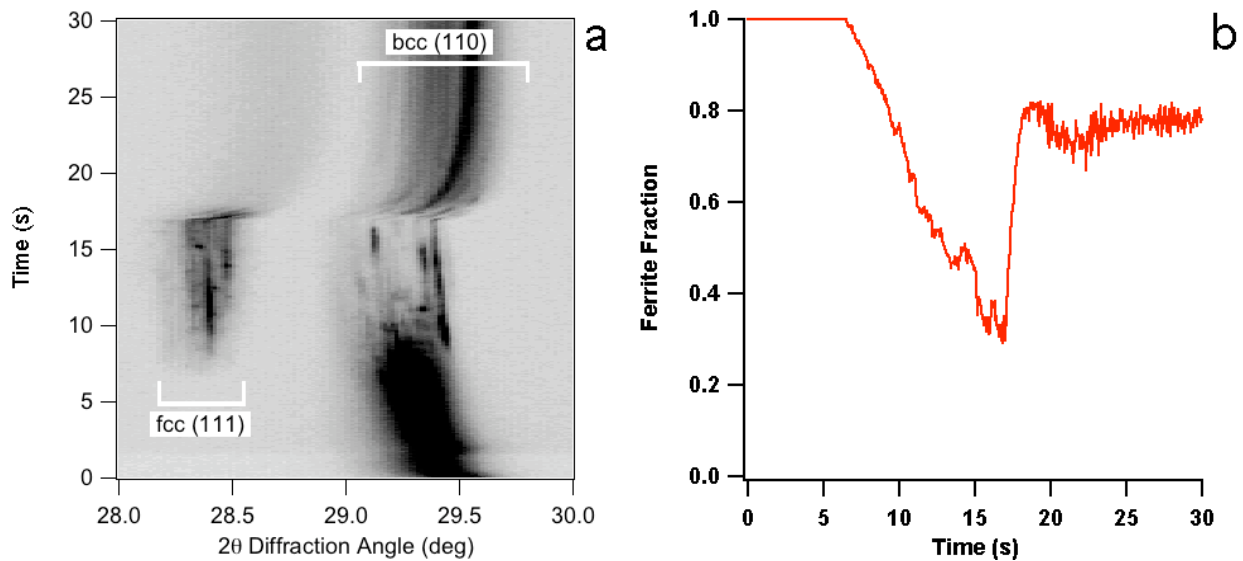


Fig. 4 Summary of TRXRD measurements from the HAZ of Fe-C-Al-Mn steel: (a) the diffraction intensity as a function of 2θ and time and (b) variation of ferrite fraction as a function of time.

The rate of ferrite decomposition was calculated using DICTRA software [1]. The geometry and conditions used for the simulation are shown in Fig. 5. In this case, the room-temperature microstructure is taken as a mixture of ferrite and 14% martensite based on optical microscopy analysis. The carbon concentration of ferrite was set at 0.03 wt %, based on thermodynamic calculations at 800 K. The carbon concentration of martensite (here represented by supersaturated ferrite) was based on the nominal composition and ferrite fraction. The simulations were performed with a simulated thermal cycle. The thermal cycle consists of two-stage heating, first a rapid heating from 800K until 1510 K at a rate of 100 K/s and then slow heating (1 K/s) to 1520 K. This is similar to the predicted temperature cycle for the current welding condition using a computational heat-transfer and fluid flow model [30]. In these diffusion controlled growth calculations, the initial microstructure was assumed to be free of cementite.

The phase diagram [see Fig. 6a] calculations show that the Fe-C-Al-Mn steel used in this investigation would never transform to 100% austenite on heating. This is in contrast to a Fe-C-Mn steel, in which the room-temperature ferrite-pearlite microstructure transforms to 100% austenite [44]. The DICTRA simulations are in qualitative agreement with the observed transformation kinetics and proved the applicability of these models for predicting the

microstructure in welds. The calculations also show that the predictions and the TRXRD observations are far from the ferrite predicted by equilibrium conditions.

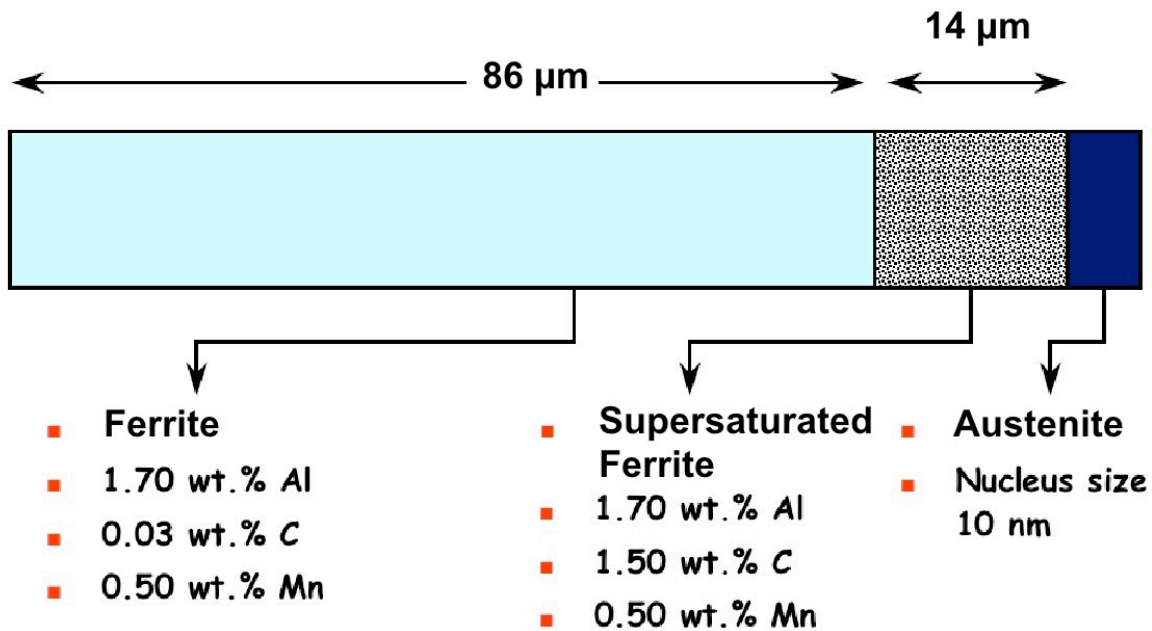


Fig. 5: Schematic illustration of the simulation geometry and boundary conditions used in diffusion-controlled calculation of austenite formation and growth in the HAZ of the weld.

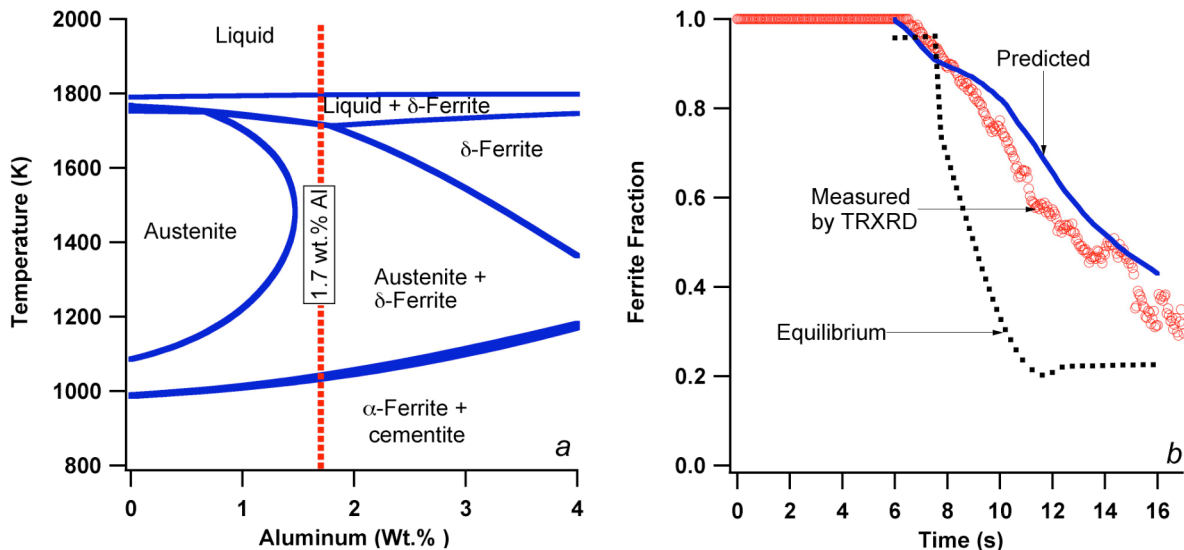


Fig. 6 (a) Pseudo binary phase diagram shows the stability of different phases in Fe-C-Al-Mn steel. (b) Comparison of measured ferrite fraction with predicted ferrite fraction for a typical heating cycle experienced by the HAZ and also the equilibrium ferrite fraction.

Dynamics of the Phase Evolution in Fusion Zone

As per the phase diagram shown in Fig. 6a, the liquid should solidify first as ferrite in this Fe-C-Al-Mn steel. In addition, with the presence of ferrite in the HAZ [see Fig. 4], the epitaxial solidification of δ -ferrite dendrites is expected. Therefore, the expected result is the emanation of **bcc** diffraction peaks first from the liquid.

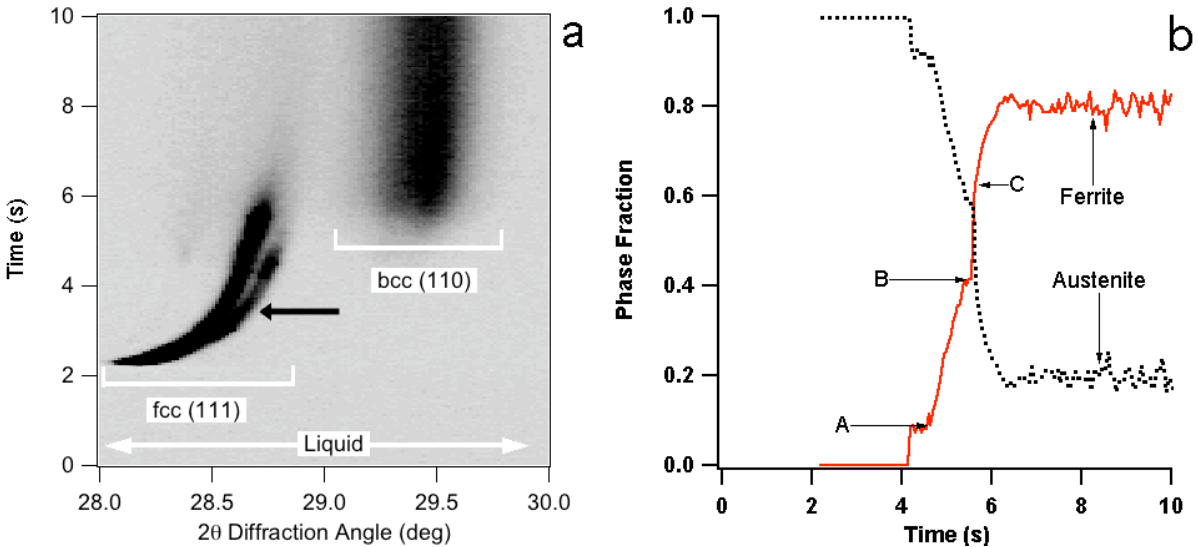


Fig. 7 Summary of TRXRD measurements from the FZ of Fe-C-Al-Mn steel: (a) the diffraction intensity as a function of 2θ and time, which shows the formation of austenite first from the liquid. The zero time in the x-axis corresponds to the arc extinction. The arrow shows evidence for the austenite peak splitting (b) Variation of phase fractions as a function of time during weld cooling is shown.

TRXRD experiments were performed to observe this behavior, and the results from the FZ are shown in Fig. 7. When the arc was on, the FZ contains only liquid and no diffraction was observed. The data collection started as soon the arc was shut off. Within 2 seconds of the arc shut-off the diffraction peaks appeared. In contrast to the theoretical prediction of ferrite formation first, the experimental results showed the formation of austenite (**fcc**) first from the liquid. With continued cooling, the **fcc** diffraction peaks move towards higher 2θ due to the decrease in lattice parameter. Interestingly, at around 3 seconds, the **fcc** peaks also appear to be split into two distinct peaks. Continued cooling led to the emanation of **bcc** peaks followed by the disappearance of the **fcc** peaks at high- 2θ (low d-spacing) first. Subsequently the the **fcc** peak intensity at low- 2θ (high d-spacing) reduced with further increase in the intensity of **bcc** diffraction peaks. The analysis of the **bcc** diffraction peaks showed three distinct kinetic stages [see Fig. 7b]. First stage transformation starts at about 4s (marked as A) and continues until 4.25 s. The second stage of transformation starts at 4.5 s and completes at 5.4 s (marked by B). The third stage starts at 5.55s and continues until 6.3s. These three stages are tentatively attributed to the three different ferrite morphologies i.e., allotriomorphic ferrite (A), bainite (B) and martensite (C) observed in the fusion zone microstructure [see Fig. 3b].

The appearance of **fcc** diffraction peaks first indicated that the nonequilibrium solidification of liquid into austenite has occurred. It is indeed interesting to note that the austenite formation is promoted even with the presence of high-concentrations of aluminum. The phase selection of austenite instead of ferrite during rapid liquid-solid interface velocity is a well-known phenomenon in stainless steel welds [9]. However, such a transition in low-alloy steel has never been reported since the solid-solid phase transformation at low-temperature often destroys the austenite that forms during solidification.

To evaluate the kinetic feasibility of solidification of austenite in Fe-C-Al-Mn welds, calculations were performed with an interface response function model [9,31]. By using this model, the liquid- δ -ferrite interface and liquid-austenite interface temperatures can be estimated

as a function of interface velocity. If the temperature of the liquid- δ -ferrite interface is higher than that of the liquid-austenite interface, one can conclude that the liquid- δ -ferrite interface will lie ahead of the liquid - austenite interface. In other words, this will suggest a primary mode of solidification by δ -ferrite. The opposite will be true for the primary mode of solidification by austenite.

Initial analyses showed that, using published Gibbs Thompson coefficient parameters [Γ] for the stainless steels [9], the transition from ferrite to austenite mode of solidification is not possible in these steels. However, by arbitrarily changing the value of Γ for ferrite from 2.6×10^{-7} to 2.6×10^{-6} , the ferrite interface temperature could be reduced to a temperature below that of austenite. With these new calculations [see Fig. 8], the austenite dendrite-tip interface would lie ahead of the ferrite dendrite-tip interface, resulting in an austenitic mode of solidification at high solidification rates. This is in agreement with experimental observations. Furthermore, these calculations also show that at low velocities, the ferrite will be the primary phase, which has also been experimentally proven [31]. Although this finding is in agreement with experimental measurement, future work is needed to rationalize the selection of an appropriate Gibbs Thompson coefficient (Γ) [45].

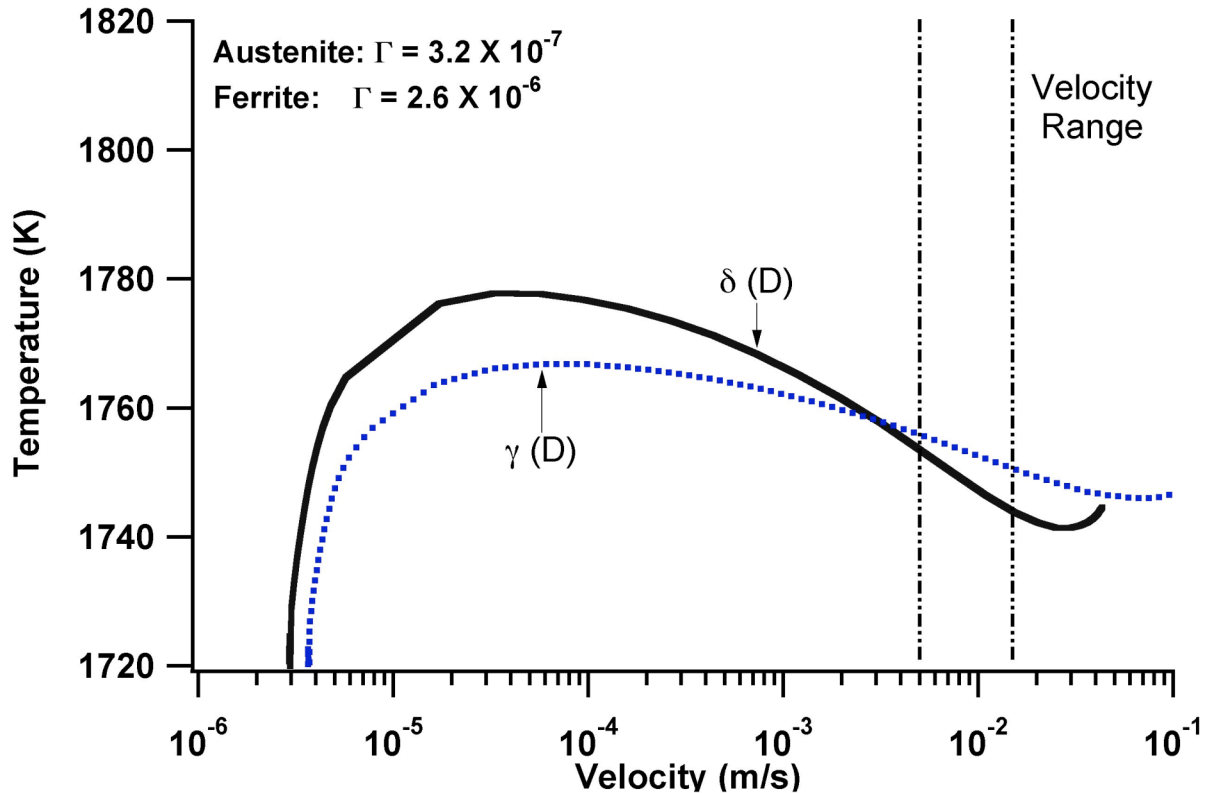


Fig. 8 Predicted variations of liquid- δ -ferrite and liquid- γ -austenite interface temperatures for dendritic (D) growth as a function of interface velocity with modified Γ value for δ -ferrite and the velocity range for the current experimental conditions.

The above example shows that the TRXRD observations can help us to monitor nonequilibrium phase selection in welds. At the same time, the splitting of the austenite peak was observed during cooling and this was not examined further in the earlier work [31]. However, this result will be discussed with the context of low-temperature decomposition of austenite to bainite in high-carbon steels in the next section.

Low-Temperature Decomposition of Austenite to Bainite in high-carbon steels

In this research, the rate of austenite decomposition during continuous cooling and isothermal decomposition was tracked under controlled heating and cooling conditions [46] in a high-carbon bainitic steel [32,33]. The chemical composition of the steel is Fe-0.75C-1.63Si-1.95Mn-0.29Mo-1.48Cr-0.1V-0.01Al-0.003P-0.003S wt%. This steel was selected because, the austenite to bainitic ferrite transformation rate is slow due to a high carbon concentration and there are no other transformations including carbide precipitation that interfere with the formation of the bainitic ferrite. The focus of the experiment was to monitor the transformation kinetics as well as the diffraction peak shape and position as a function of temperature and time. The samples were heated to 1273 K and held at that temperature for 4 minutes. In the continuous cooling experiment, the sample was cooled at a nominal rate of 10 K/s from 1273 K to room temperature. In the isothermal experiments, the samples were cooled at a rate of 10 K/s from 1273 K to 573 K and held at that temperature for 12 hrs. The temperature was controlled using direct resistive-heating using a type S (Pt/Pt10%Rh) thermocouple. Covering the sample with an inverted can filled with He reduced the oxidation of samples.

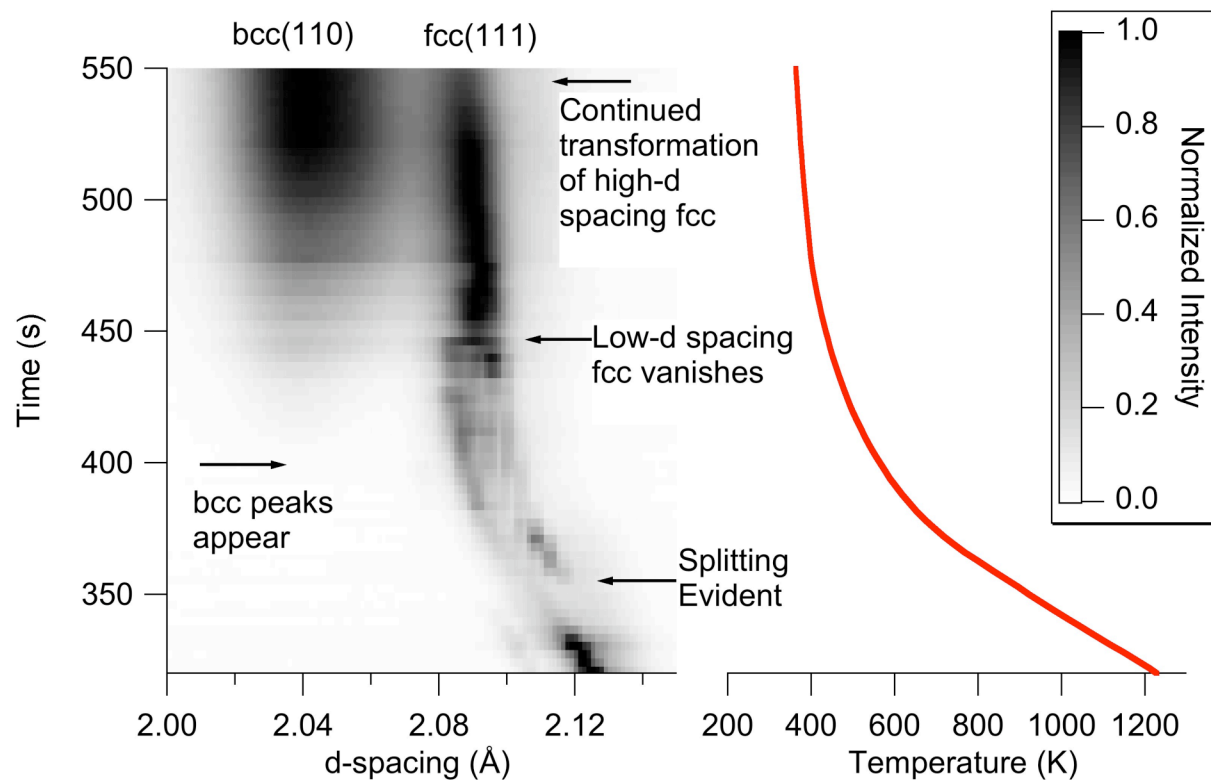


Fig. 9 Measured intensities of **bcc** (110) and **fcc** (111) diffraction peaks in the image format as a function of d-spacing and time and corresponding temperature variation are shown for continuous cooling experiment.

Continuous Cooling Experiments

In-situ X-ray diffraction observations were performed during controlled cooling conditions at different rates. In the first experiment, the steel sample was cooled at a rate of 10 K/s at elevated temperatures. However, due to the absence of forced air-cooling, the cooling rate dropped to 1 K/s below 673 K. The measurements [see Fig. 9] showed that, on cooling below

873 K, the **fcc** diffraction peaks appear to split into two distinct peaks with a small and large d-spacing. On further cooling, to 673 K, the **bcc** diffraction peaks begin to appear and the intensity of low-d spacing **fcc** peaks reduces. With continued cooling, the splitting of **fcc** diffraction peaks gradually vanishes and the peaks become more broadened. Continued cooling to room temperature lead to gradual decrease of **fcc** diffraction peaks with corresponding increase in **bcc** diffraction intensity. This measurement of **fcc** diffraction peak splitting in this experiment is similar to the peak splitting observed in the fusion welded region shown in Fig. 7.

Isothermal Experiments

In this experiment, the steel sample was cooled at a rate of 10 K/s to 573 K from 1273 K and held isothermally for 12 hrs. It is important to note that these experiments were performed before the continuous cooling experiments. The results from two samples are summarized in Fig. 10. The images show changes in the diffraction patterns during the isothermal hold at 573 K from 10 to 30000 s. For sample 1, the image [see Fig 10a] shows only **fcc** (111) diffraction in the early stages of the isothermal heat treatment.

This shows that the sample is fully austenitic on reaching 573 K. With increasing time at 573 K, the width of the **fcc** (111) peak increases and the intensity distribution becomes bimodal at the point indicated by the arrow “A1” in the plot. This occurs before any detectable transformation to ferrite. Ferrite eventually appears, as indicated by the faint diffracted intensity from **bcc** (011) peaks [see arrow F1]. Continued holding leads to a rapid increase in ferrite fraction [see arrow F2] and eventual elimination of splitting in the austenite peak [see arrow A2].

In sample 2, the image [see Fig. 10b] shows a **fcc** (111) diffraction peak and a weak **bcc** (011) diffraction very faint peak [see arrow F1] at the early stages of heat-treatment. The width of the

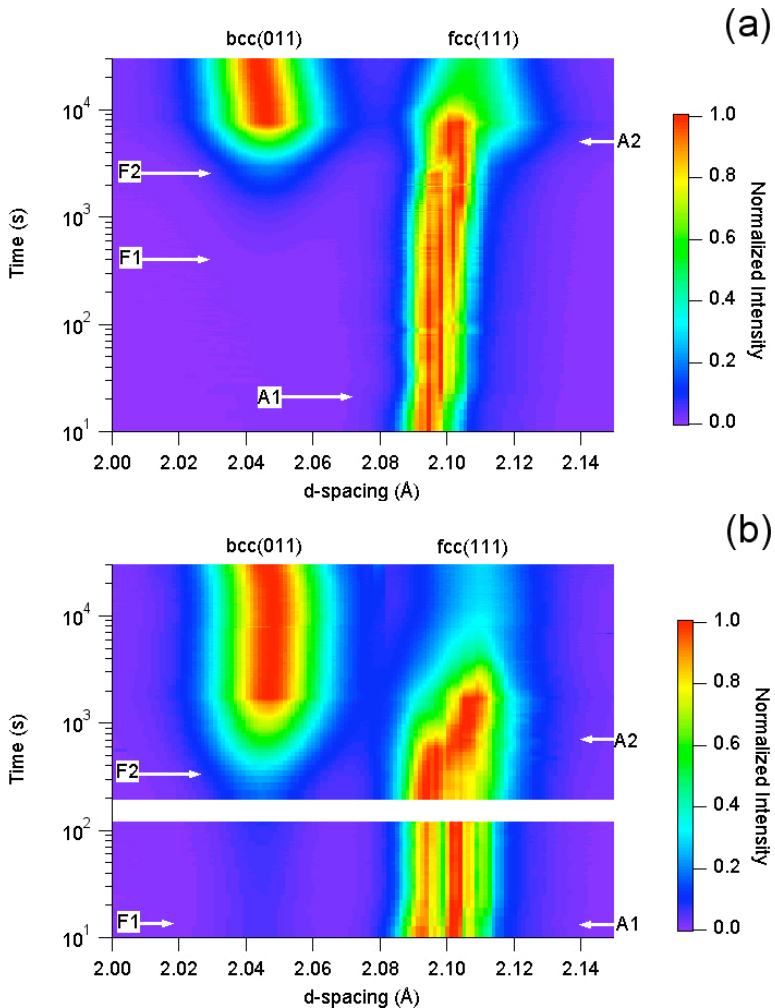


Fig. 10 Image representations of diffraction data from two samples subjected to isothermal heat treatments. In this image, the blue color corresponds to the background intensity and the maximum intensity is given by the red color. (a) Sample 1 which shows ferrite transformation only after reaching isothermal temperature: (b) Sample 2: The blank white region in the image corresponds to absence of measurement due to a change in integration time. In this experiment the extent of splitting is large and also there is some ferrite formation during cooling.

fcc (111) diffraction peak is large [see arrow A1] and has a bimodal intensity distribution (peak “splitting”).

Analysis showed that the splitting of **fcc** (111) peaks occurred during cooling from high temperatures to the isothermal transformation temperature. At longer times at 573 K, the intensity of the **bcc** diffraction peaks increased and the positions of the **fcc** diffraction peaks moved towards higher interplanar spacing. The lattice parameter of the austenite became more uniform as the ferrite fraction increased, as shown by arrows “A2” and “F2” in the images, respectively. The kinetics of ferrite fraction in sample 1 is less rapid than that of sample 2. Optical microscopy of samples after the isothermal transformation showed the existence of bainitic microstructure and some untransformed austenite [46]. In summary, both the results show the tendency for the **fcc** diffraction peak to split into two distinct peaks at the early stages and become more uniform and broad as the ferrite fraction increases. In addition, they also show the variability involved in the extent of peak splitting. The tendency for splitting of **fcc** (111) diffraction peaks in sample 1 after reaching 573 K and before the initiation of ferrite is evaluated further.

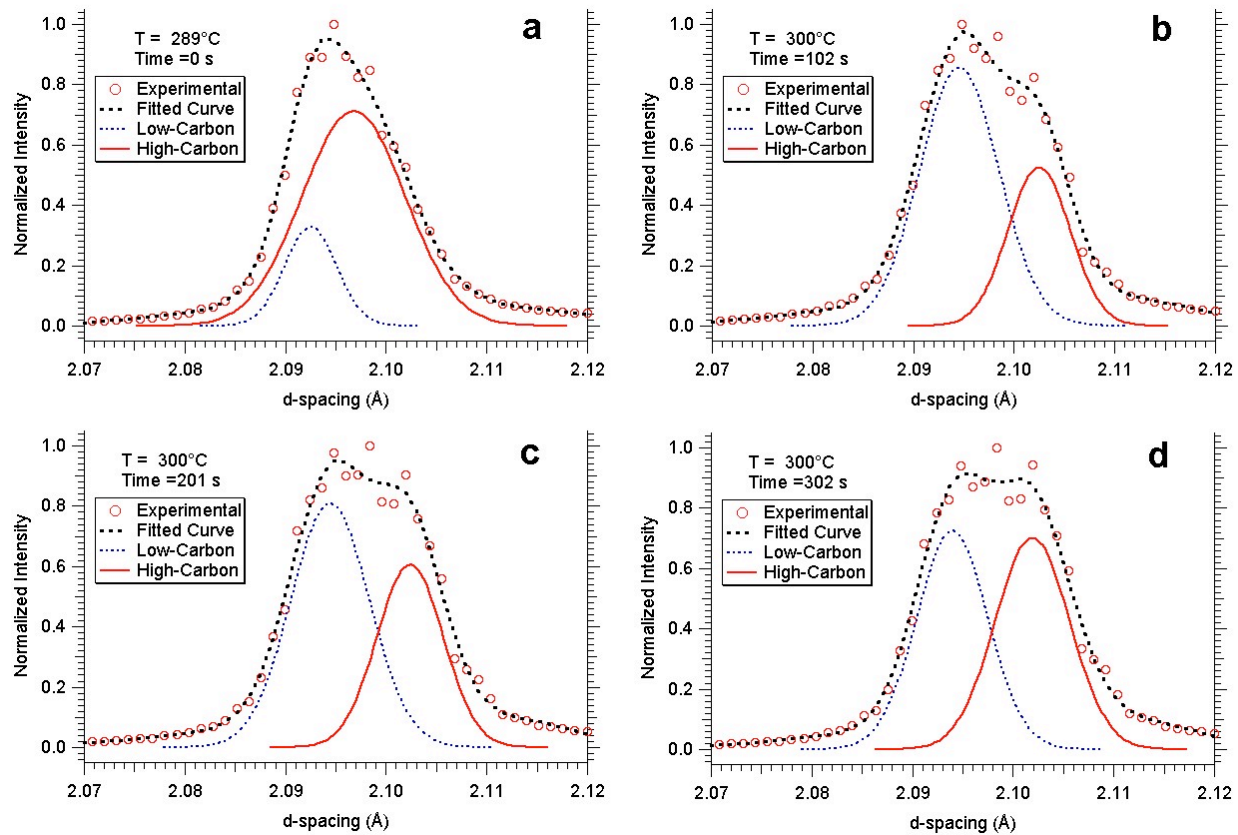


Fig. 11 Analyses of **fcc** (111) diffraction peaks measured at different time intervals from sample 1 during isothermal holding at 573 K is shown with the fitted peaks with a Gaussian peak shape. (a) The diffraction peaks from 0 second shows the onset of peak splitting and the temperature is 562 K. Diffraction peaks at (b) 102, (c) 201 and (d) 302 seconds into isothermal hold at 573 K showing the onset and development of peak splitting.

From the published relationship [47] between the austenite composition and lattice parameter at room temperature (300 K) (a_{FCC}), the carbon concentration has the largest contribution.

$$d_{\{111\}}^{FCC} = a_{FCC} / \sqrt{3}$$

$$a_{FCC} = 3.5780 + 0.033x_c + 0.00095x_{Mn} - 0.0002x_{Ni} + 0.0006x_{Cr} + 0.0056x_{Al} + 0.0031x_{Mo} + 0.0018x_V \quad (1).$$

In the above equation x_i corresponds to the weight percent of elements “ i ” in the austenite. Since the mobility of the substitutional elements at 573 K is low, the dynamics of austenite peak splitting is interpreted as the development of carbon-rich and carbon-poor austenite regions. In addition, the carbon concentration of the ferrite was also estimated using the relation between ferrite composition and lattice parameter [46].

To evaluate the peak splitting of austenite further, the peak shape and area fraction analyses were performed using numerical methods. The summary of the results is presented in Fig. 11. The peak shape analysis showed that the **fcc** (111) diffraction peak had a tendency to separate into two distinct peaks [see Fig. 11]. It is important to note that the tendency for peak splitting is very weak at 0-s and the peak fitting may not be reliable. In contrast, with continued isothermal holding, this tendency to split into two distinct peaks became stronger [see Fig. 11b to 11d] and the results from peak fit analysis are consistent.

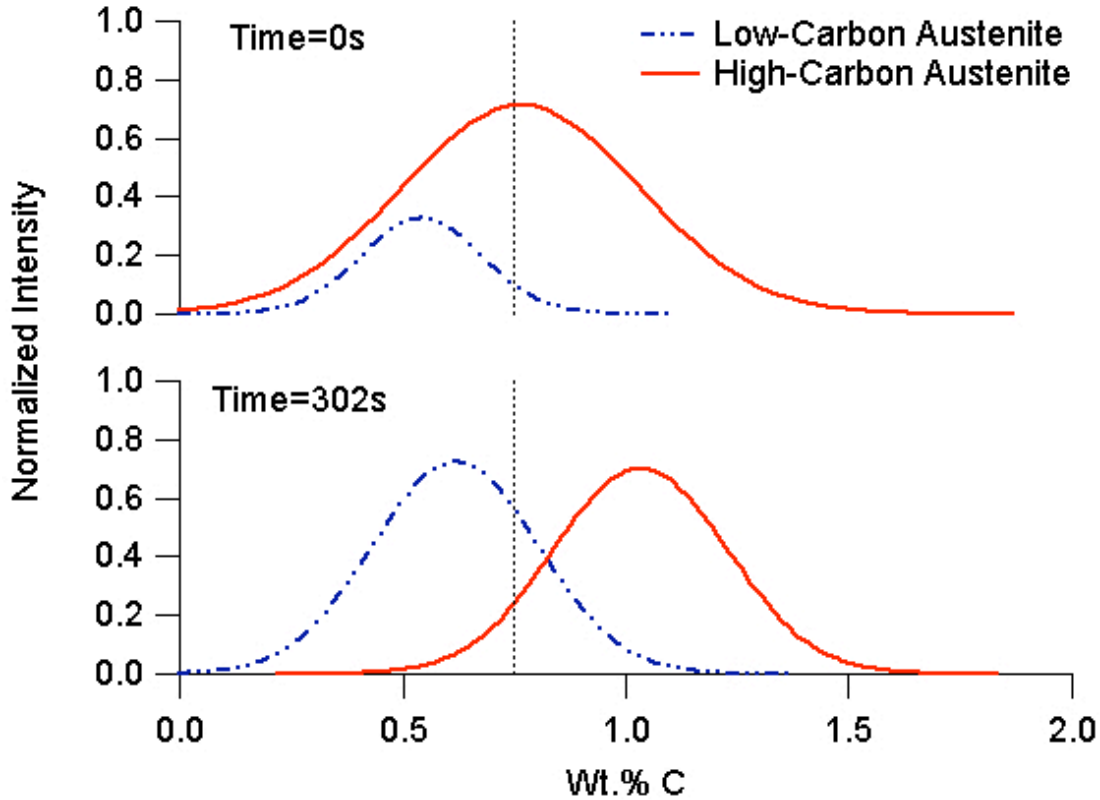


Fig. 12 Comparison of the measured diffracted intensities from low- and high-carbon austenite at time 0- and 302-seconds at 573K as a function of estimated carbon concentration.

Using the peak analysis, the carbon concentrations of the two types of austenite can be estimated if it is assumed that lattice parameter variations are only due to carbon variations. Using the measured thermal expansion coefficient for austenite ($2.5032 \times 10^{-5} \text{ K}^{-1}$), the lattice parameters at 573 K were calculated and the carbon concentrations of these two austenite regions were deduced from equation (1) at different time intervals [see Fig. 12]. Since the peak positions of the two austenite regions lie [see Fig. 12] on either side of the bulk carbon concentration, the

interpretation of the austenite splitting as the formation of two different austenite regions with low- and high-carbon concentration appears to be valid. The separation of austenite into a two-phase region before the bainitic transformation is indeed intriguing. Other researchers have postulated the existence of pre-cursor events in austenite before its decomposition to bainitic ferrite [54–59].

Consideration of Factors for Austenite Peak Splitting behavior

The above results and analyses indicated the separation of austenite [see Fig. 11] into two different regions with different lattice parameters. This was tentatively interpreted as the formation of low-carbon and high-carbon regions. However, this interpretation needs to be evaluated in the context of other possible effects.

(i) The lattice parameter of austenite also depends on substitutional solutes [Equation 1]. Any variation in substitutional solute content could, in principle, lead to corresponding changes in the austenite lattice parameter. The energy dispersive X-ray peak intensity mapping [46] analyses of the samples showed no significant long-range heterogeneity. Substitutional atom might diffuse via some sort of a spinodal reaction within the 400 s of the observed lattice parameter fluctuations at 573 K. The estimated diffusion distance for substitutional atoms for 400 s at 573 K in austenite is 1×10^{-14} to 1×10^{-13} m, which is less than the interatomic distance. In contrast, the diffusion distance for carbon atoms is expected to be 36 nm. Therefore, the observed austenite diffraction peak splitting after reaching 573 K cannot be attributed to diffusion of substitutional atoms.

(ii) Carbon concentration gradients may develop if carbides precipitate from the austenite during cooling from austenitizing temperature. However, the alloy is designed with high silicon content, precisely to avoid carbides. Extensive electron microscopy and atom probe microscopy analysis of the same steel has demonstrated the absence of carbides in the microstructure [33].

(iii) Decarburization from the surface of the sample contributing to carbon variations in the austenite as a function of depth is of concern for the current experiment. However, careful optical microscopy and hardness measurements failed to show any decarburization. Furthermore, decarburization should lead to a continuous variation of carbon content and not to the formation of two distinct austenite diffraction peaks. Therefore, decarburization is expected to produce austenite peak broadening and reduction of lattice parameter, which is not observed in this case.

(iv) It is important to consider the size of the austenite grains as well as stress and strains. A particle of size L will give a diffraction peak width $w=0.6d^2/L$; $w_{111}=0.01 \text{ \AA}$ corresponds to $L=260 \text{ \AA}$. While ferrite would be expected to nucleate with a small particle size within the austenite, there is no reason to expect such a dramatic decrease in the austenite particle size in the early stages of transformation. An inhomogeneous stress distribution with Gaussian width w_{stress} will give peak width $w=w_{\text{stress}}d/G$, where $G=75 \text{ GPa}$ is the shear modulus of austenite. $w_{111}=0.01 \text{ \AA}$ corresponds to $w_{\text{stress}}=360 \text{ MPa}$. Transformation stresses might be this large in the small fraction of ferrite, but not in the bulk of the austenite. However, during the formation of plate shaped ferrite, the strains can be accommodated entirely in the austenite [60]. These strains will not be uniform, increasing with magnitude as the plate shape is reached. In any cases, these two sources of *broadening* would not be expected to produce a peak *splitting*.

Since the above effects do not support the peak splitting, in the following section possible mechanisms for the development of carbon-rich and carbon-poor regions are discussed.

(a) A possible cause of carbon partitioning in austenite is spinodal decomposition. A solid solution can become heterogeneous by spinodal decomposition, if the enthalpy of solution is such that it favors the clustering of like atoms. In these circumstances, the free energy of mixing can show two minima as a function of concentration, leading to the possibility of spinodal decomposition at low temperatures. Although, theoretical analyses based on computational thermodynamic calculations [1,46, 61] showed that spinodal decomposition of austenite is not possible for the current steel, we need to evaluate the thermodynamic description of austenite as a function of carbon at low-temperature.

(b) Another possibility is the classical two electronic states model for austenite, in which there is co-existence of high and low molar volume states of austenite at any temperature with high- and low-magnetic moment. The apparently large thermal expansion coefficient of austenite is because the fraction of each state is temperature dependent [62]. If carbon were to segregate to the high-volume state (with more room for interstitial atoms), the effects of magnetism and interstitial carbon could synergistically lead to decomposition of austenite into a high-volume, high-moment, high-carbon and a low-volume, low-moment, low carbon phase. The measured diffraction intensities of two different austenite regions were compared with theoretical estimate of low- and high-volume lattice parameters in Fig. 13. It is interesting to note that the current measurement lie in between these two bounds. This proposed hypothesis requires further work in alloys without the interference of ferrite precipitation and effect two-gamma states on the free energy of austenite at low temperature must be evaluated allowing for carbon partitioning [63].

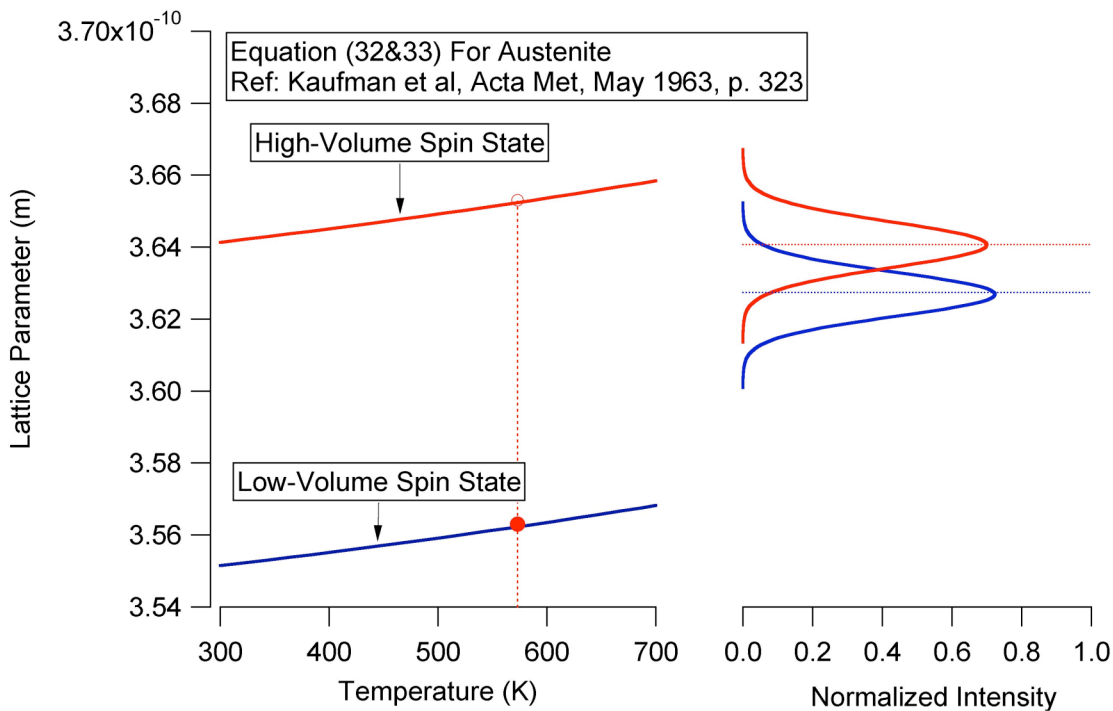


Fig. 13 Comparison of the measured diffracted intensities from low- and high-volume austenite region with theoretical estimate of lattice parameter for low- and high-volume austenite by Kaufman et al [62].

Future Directions

The above examples showed the power of in-situ synchrotron diffraction technique to explore the mechanisms of phase transformations in real-time rather than post-experimental evaluation where the high-temperature effects are lost. This is indeed valuable for nonequilibrium conditions where the transformations may deviate from the expected behavior. In addition, this tool in conjunction with ex-situ characterization techniques including electron microscopy and atom probe field ion microscopy, can lead to a better understanding of interactions between different physical processes including lattice stability and atomic mobility in complex structural alloys. With further developments in detectors and analysis methodologies [18,19,64], it is possible to explore the kinetics of phase stability, as well as the morphology of phases, in greater details under in-situ conditions. In addition, it is possible to explore the interaction of stress and temperature on phase transformation in different crystallographic axes [65]. Furthermore, we can employ these tools to understand the effects of multiple thermal cycles, and thereby understand the role of initial microstructures on subsequent phase transformation [66]. Although, these in-situ characterization tools are powerful, there is a challenge to develop robust analytical methods to deconvolute competing physical processes.

Summary

The transition from equilibrium to nonequilibrium microstructure evolution in structural alloys is an inherent part of manufacturing processes including welding and heat-treatment. Research in the past 10 years has demonstrated that the time-resolved scattering technique using synchrotron radiation and high-flux neutrons is an ideal tool to characterize these transitions. In this paper, the power and applicability of time-resolved X-ray diffraction technique using synchrotron radiation were demonstrated through in-situ characterization of the microstructure evolution during welding of Fe-C-Al-Mn steel and of the bainitic transformation a high-carbon steel.

The growth of austenite in the heat-affected-zone of Fe-C-Al-Mn steel was tracked using time-resolved X-ray diffraction technique. The results showed incomplete austenitization because of increased phase stability of ferrite caused by a large (> 1 wt %) aluminum concentration. This microstructure was in agreement with computational thermodynamic and kinetic calculations. In contrast, a transition from equilibrium δ -ferrite solidification to non-equilibrium austenite solidification was observed in the fusion zone due to rapid cooling. The changes in the primary mode of solidification with the change in cooling rate were evaluated by coupling interface response function models with thermodynamic calculations.

Transformation kinetics and lattice parameters were measured *in-situ* during isothermal transformation of a high-carbon austenite to bainitic ferrite using the time-resolved X-ray diffraction technique. The analyses of **fcc** diffraction peaks indicated splitting of these peaks before the appearance of **bcc** diffraction peaks. The observed splitting was interpreted as the separation of austenite into a carbon-poor and carbon-rich austenite. The fraction of low-carbon austenite region gradually decreased with the onset of the bainitic ferrite transformation. With continued isothermal holding, as the decomposition of high-carbon austenite to ferrite also progressed. With continued transformation to ferrite the austenite peak shape became more uniform and the position shifted to larger lattice parameter.

Acknowledgements

Research was sponsored by the Division of Materials Sciences and Engineering, U. S. Department of Energy, under Contract DE-AC05-00OR22725 with UT-Battelle, LLC. The UNICAT facility at the Advanced Photon Source (APS) is supported by the U.S. DOE under Award No. DEFG02-91ER45439, through the Frederick Seitz Materials Research Laboratory at

the University of Illinois at Urbana-Champaign, the Oak Ridge National Laboratory (U.S. DOE contract DE-AC05-00OR22725 with UT-Battelle LLC), the National Institute of Standards and Technology (U.S. Department of Commerce) and UOP LLC. The APS is supported by the U.S. DOE, Basic Energy Sciences, Office of Science under contract No. W-31-109-ENG-38. Part of the phase selection work is supported under the auspices of the U. S. Department of Energy, Lawrence Livermore National Laboratory, under Contract No. W-7405-ENG-48. The authors thank Drs. O. Barabash and J. Pang for helpful discussions on the paper.

References

1. J. -O. Andersson et al., "Thermo-Calc and DICTRA, Computational tools for materials science," *CALPHAD*, 26 (2002) 273 – 312.
2. S. S. Babu, S. A. David, and M. A. Quintana, "Modeling microstructure development in Self-Shielded Flux Cored Arc Welds," *Welding Journal*, 80 (2001) 98s-105s.
3. S. S. Babu et al., "Characterization of the microstructure evolution in a nickel base superalloy during continuous cooling conditions," *Acta Materialia*, 49 (2001) 4149 - 4160
4. S. S. Babu et al., "Solidification and microstructure modeling of welds in aluminum alloys 5754 and 6111," *Science and Technology of Welding and Joining*, 6 (2001) 31-40
5. J. M. Vitek, S. A. Vitek and S. A. David, "Numerical modeling of diffusion-controlled phase-transformation in ternary-systems and application to the ferrite austenite transformation in Fe-Cr-Ni system," *Metall. Mater. Trans. A.*, 26 (1995) 2007 - 2025
6. S. S. Babu et al., "Phase Stability and atom probe field ion microscopy of type 308 CRE stainless steel weld metal," *Metall. Mater. Trans. A.*, 27A (1996) 763 - 774
7. H. I. Aaronson, H. A. Domain and G. M. Pound, "Thermodynamics of the austenite to pro eutectoid ferrite transformation II, Fe-C-X alloys," *Trans. Met. Soc – AIME*, 236 (1966) 768 - 781
8. H. K. D. H. Bhadeshia, "Diffusional formation of ferrite in iron and its alloys," *Progress in Materials Science*, 29 (1985) 321 - 386
9. S. Fukumoto and W. Kurz, "Solidification phase and microstructure selection maps for Fe-Cr-Ni alloys," *ISIJ International*, 39 (1999) 1270 - 1279
10. J. Odqvist, B. Sundman and J. Agren. "A general method for calculating deviation from local equilibrium at phase interfaces," *Acta Materialia*, 51 (2003) 1035 - 1043
11. J. W. Elmer et al., "Analysis of heat-affected-zone phase transformations using in-situ spatially resolved X-ray diffraction with synchrotron radiation," *Metall. Mater. Trans. A.*, 27 (1996) 775 - 783
12. J. W. Elmer, J. Wong, and T. Ressler, "Spatially resolved X-ray diffraction phase mapping and $\alpha \rightarrow \beta \rightarrow \alpha$ transformation kinetics in the heat-affected zone of commercially pure titanium arc welds," *Metall. Mater. Trans. A.*, 29 (1998) 2761 – 2773
13. J. W. Elmer, J. Wong, T. Ressler, "In-situ observations of phase transformations during solidification and cooling of austenitic stainless steel welds using time-resolved x-ray diffraction," *Scripta Materialia*, 8, (2000) 751 – 757
14. S. S. Babu et al., "In situ observations of non-equilibrium austenite formation during weld solidification of an Fe-C-Al-Mn low-alloy steel," *Proc. Roy. Soc. A., Math. Phys. Eng.*, 2020 (2002) 811 -821
15. T. A. Palmer, J. W. Elmer, and S. S. Babu, "Observations of ferrite/austenite transformations in the heat affected zone of 2205 duplex stainless steel spot welds using time resolved X-ray diffraction," *Mater. Sci. Engg. A.*, 374 (2004) 307-321
16. C. Notthoff, et al., "Direct determination of metastable phase diagram by synchrotron radiation experiments on undercooled metallic melts," *Physical Review Letters*, 86 (2001) 1038 - 1041

17. A. Royer, P. Bastie and M. Veron, "In-situ determination of the γ' phase volume fraction and of relations between lattice parameters and precipitate morphology in Ni-based single crystal superalloy," *Acta Materialia*, 46 (1998) 5357 - 5368
18. S. E. Offerman, et al., "Grain nucleation and growth during phase transformations," *Science* 298 (2002) 1003 – 1005
19. S. Chmidt et al., "Watching the growth of bulk grains during recrystallization of deformed metals," 305 (2004) 229 – 232.
20. S. E. Offerman et al., "Solid-state phase transformations involving solute partitioning: modeling and measuring on the level of individual grains," *Acta Materialia*, 54 (2004) 4757 – 4766.
21. S. E. Offerman et al., "In-situ study of pearlite nucleation and growth during isothermal austenite decomposition in nearly eutectoid steel," *Acta Materialia*, 51 (2003) 3927 – 3938
22. G. Bruno and H. C. Pinto, "Precipitation kinetics of γ' phase in nickel base superalloy SC16: an in situ neutron diffraction study," *Materials Science and Technology*, 19 (2003) 567 – 572
23. Advanced Photon Source: <http://www.aps.anl.gov/>
24. ESRF - The European Synchrotron Radiation Facility: <http://www.esrf.fr/>
25. Stanford Synchrotron Radiation Laboratory: <http://www-ssrl.slac.stanford.edu/>
26. ISIS: <http://www.isis.rl.ac.uk/>
27. Spallation Neutron Source: <http://www.sns.gov/>
28. Lujan Neutron Scattering Center: <http://lansce.lanl.gov/lujan/index.html>
29. J. Wong et al., "Time-resolved X-ray diffraction study of solid combustion reactions," *Science*, 249 (1990) 1406 - 1409
30. S. S. Babu et al., "Modeling and characterization of nonequilibrium weld microstructure evolution," *Proc. Mathematical Modeling of Weld Phenomena 7*, (2004) Graz, Austria
31. S. S. Babu et al., "Time-resolved X-ray diffraction investigation of primary weld solidification in Fe-C-Al-Mn steel welds," *Acta Materialia*, 50 (2002) 4763-4781
32. F. G. Caballero et al., "Very strong low temperature bainite," *Materials Science and Technology*, 18 (2002) 279 - 284
33. M. Peet et al., "Three-dimensional atom probe analysis of carbon distribution in low-temperature bainite," *Scripta Materialia*, 50 (2004) 1277-1281
34. V. Karpenko, et al., "Beamline-10 - a multipole wiggler beamline at SSRL," *Review of Scientific Instruments*, 60 (1989) 1451-1456
35. A. P. Hammersley et al., "Two-dimensional detector software: From real detector to idealised image or two-theta scan," *High Pressure Research*, 14 (1996) 235-248
36. J. W. Elmer et al., "In-situ observations of lattice expansion and transformation rates of α and β phases in Ti-6Al-4V," *Materials Science and Engineering A*, 391/1-2 (2005) 104 – 113
37. B. Sundman, B. Jansson, and J. O. Andersson, "The Thermo-Calc databank system," *Calphad*, 1985, **9**, pp. 1-153.
38. SGTE Solution Database (1992) Editor: B. Sundman, Division of Computational Thermodynamics, Royal Institute of Technology, Stockholm, Sweden.
39. W. Kurz, B. Giovanala, and R. Trivedi, "Theory of microstructural development during rapid solidification," *Acta Metall*, 1986, **34**, pp. 823-830.
40. M. J. Aziz, "Model for solute distribution during rapid solidification," *J. Appl. Physics*, 1982, **53**, pp. 1158-1168.
41. O. Hunziker, "Theory of plane front and dendritic growth in multicomponent alloys," *Acta Mater.*, 2001, **49**, pp. 4191-4203.

42. R. Trivedi and W. Kurz, "Dendritic growth," *International Materials Reviews*, 1994, **39**, pp. 49-74.
43. O. Hunziker, M. Vandyousseffi and W. Kurz, "Phase and microstructure selection in peritectic alloys close to the limit of constitutional undercooling," *Acta Mater*, 1998, **46**, pp. 6325-6336
44. J. W. Elmer et al., "Kinetic modeling of phase transformations occurring in the HAZ of C-Mn steel welds based on direct observations," *Acta Materialia*, 2003, **51**, (2003) 3333-3349
45. R. Trivedi and W. Kurz, "Dendritic growth," *International Materials Reviews*, 39 (1994) 49-74
46. S. S. Babu et al., "In-situ observations of lattice parameter fluctuations in austenite and transformation to bainite," submitted for publication in *Metallurgical and Materials Transactions A*, 2005
47. D. J. Dyson and B. Holmes, "The effect of alloying elements on lattice parameter of austenite," *Journal of the Iron and Steel Institute*, 1970, **208**, 469
54. R. I. Entin, "The elementary reactions in the austenite->pearlite and austenite->bainite transformations," in the proceedings of Decomposition of Austenite by Diffusional Processes, Eds. V. F. Zackay and H. I. Aaronson, Interscience Publishers, New York, 1962
55. Z. Bojarski and T. Bold, "Structure and properties of carbide-free bainite," *Acta Metallurgica*, 22 (1974) 1223 – 1234
56. C. Lim and M. Wutting, "Pre-bainitic phenomena in AISI 86B80 and 0.8C-5.3Ni steel," *Acta Metallurgica*, 22 (1974), 1215 – 1222
57. J. H. Zhang, S. C. Chen and T. Y. Hsu. "An investigation of internal-friction within the incubation period of the bainitic transformation," *Acta Metallurgica*, 37 (1989) 241 - 246
58. X. L. Wu et al., "Study of carbon-poor regions of austenite during bainite incubation period by SAM," *J. Mater. Sci. Technol.*, 11 (1995) 353 – 357
59. X. L. Wu et al., "Displacive mechanism of bainite transformation in carbon-depleted region of austenite," *Materials Transactions, JIM.*, 35 (1994) 782 - 786
60. J. W. Christian, "The theory of transformations in metals and alloys – Part 1," Pergamon Press, Elsevier Science, New York, 2002, p. 461
61. Thermotech Fe-Data Thermodynamic Database, Thermotech Ltd / Sente Software Ltd., UK
62. L. Kaufman, E. V. Clougherty, and R. J. Weiss, "The lattice stability of metals – III. Iron," *Acta Metallurgica*, 11 (1963) 323 – 335
63. A. P. Miodownik and M. Hillert, "A thermodynamic treatment of the ferromagnetic transition in alloys," 4 (1980) 143 – 153
64. W. J. Liu et al., "The three-dimensional X-ray crystal microscope: A new tool for materials characterization," *Metall. Mater. Trans. A.*, 35A (2004) 1963 - 1967
65. S. S. Babu, E. A. Payzant, D. W. Brown, "Interaction of stress on phase stability in single-crystal nickel-base superalloys," Unpublished research, Oak Ridge National Laboratory, 2005
66. S. M. Kelly et al., "Measurement of phase transformation kinetics during repeated thermal cycling of Ti-6Al-4V using time-resolved X-ray diffraction," proceedings of this conference.